The impact of hydrogen bonding on amide ^{1}H chemical shift anisotropy studied by cross-correlated relaxation and liquid crystal NMR spectroscopy.

Qingdao Institute of BioEnergy and Bioprocess Technology, Chinese Academy of Sciences, Qingdao 266061; Laboratory of Chemical Physics, NIDDK, National Institutes of Health, Bethesda, MD 20892-0520; China; and National Magnetic Resonance Facility, Madison, WI 53706

Lishan Yao, Alexander Grishaev, Gabriel Cornilescu and Ad Bax

SUPPORTING INFORMATION

Full reference 47:
Frisch, M. J.; Trucks, G. W.; Schlegel, H. B.; Scuseria, G. E.; Robb, M. A.; Cheeseman, J. R.; Montgomery, J., J. A.; Vreven, T.; Kudin, K. N.; Burant, J. C.; Millam, J. M.; Iyengar, S. S.; Tomasi, J.; Barone, V.; Mennucci, B.; Cossi, M.; Scalmani, G.; Rega, N.; Petersson, G. A.; Nakatsuji, H.; Hada, M.; Ehara, M.; Toyota, K.; Fukuda, R.; Hasegawa, J.; Ishida, M.; Nakajima, T.; Honda, Y.; Kitao, O.; Nakai, H.; Klene, M.; Li, X.; Knox, J. E.; Hratchian, H. P.; Cross, J. B.; Bakken, V.; Adamo, C.; Jaramillo, J.; Gomperts, R.; Stratmann, R. E.; Yazyev, O.; Austin, A. J.; Cammi, R.; Pomelli, C.; Ochterski, J. W.; Ayala, P. Y.; Morokuma, K.; Voth, G. A.; Salvador, P.; Dannenberg, J. J.; Zakrzewski, V. G.; Dapprich, S.; Daniels, A. D.; Strain, M. C.; Farkas, O.; Malick, D. K.; Rabuck, A. D.; Raghavachari, K.; Foresman, J. B.; Ortiz, J. V.; Cui, Q.; Baboul, A. G.; Clifford, S.; Cioslowski, J.; Stefanov, B. B.; Liu, G.; Liashenko, A.; Piskorz, P.; Komaromi, I.; Martin, R. L.; Fox, D. J.; Keith, T.; Al-Laham, M. A.; Peng, C. Y.; Nanayakkara, A.; Challacombe, M.; Gill, P. M. W.; Johnson, B.; Chen, W.; Wong, M. W.; Gonzalez, C.; Pople, J. A. *Gaussian 03, Revision C.02, Gaussian Inc., Wallingford CT.*, 2004.

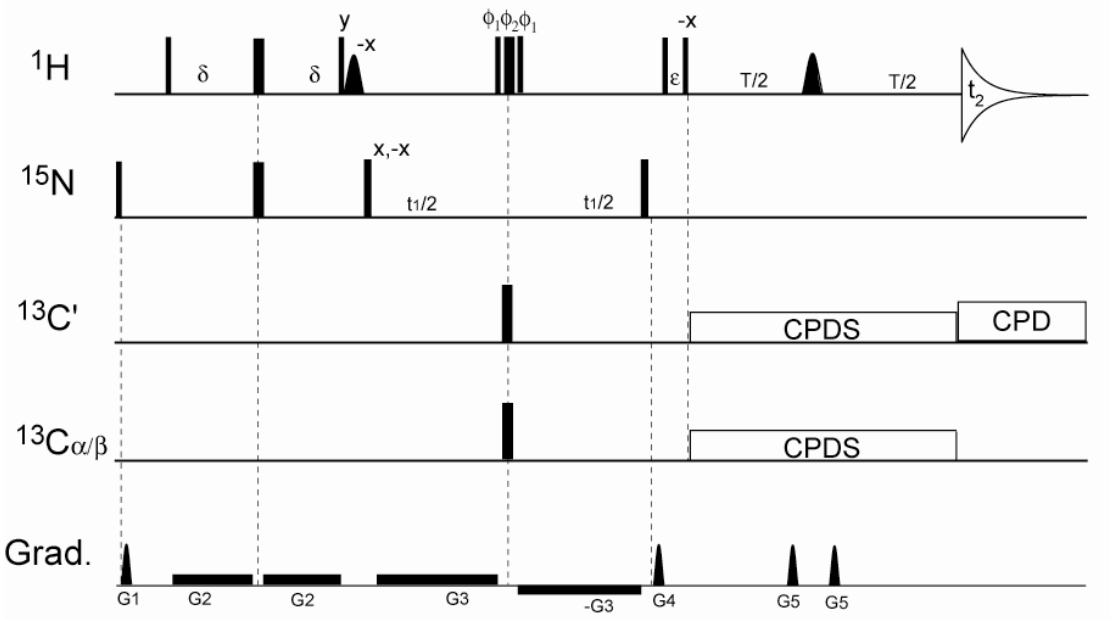

Figure S1. Pulse sequence used to measure the $^1H^N$ CSA and ^{15}N-$^1H^N$ dipole transverse cross-correlation rate, $\Gamma^{CSA,NH}$. Narrow and wide pulses correspond to 90º and 180º flip angles, respectively. All the ^{1}H pulses are centered on the H_2O resonance, at 4.75 ppm. The $^{13}C'/^{13}C^{\alpha/\beta}$ nuclei are decoupled by two rectangular pulses, centered at 177 and 55.7 ppm respectively, with durations of 47.3 μs at 600 MHz ^{1}H frequency, such that the ^{13}C' has a null at the $^{13}C^{\alpha/\beta}$ frequency, and vice versa. Protons are decoupled by the composite $90°\phi_1$-$210°\phi_2$-$90°\phi_1$ pulse. The shaped ^{1}H pulse immediately following the nonselective ^{1}H 90º pulse has a flip angle of 90º and rotates the water magnetization to $-z$ while the following gradient G3 serves to prevent radiation damping until the composite 180º pulse rotates it back to $+z$. The selective 180º ^{1}H pulse prior to acquisition is of the REBURP type (1), centered at 9.05ppm, with a duration of 1.8 ms. The phases of all pulses are x unless indicated. δ = 2.6 ms, ε = 0.097 ms. T was set to 10, 30, 50, 70, 90, 110, 130 and 150 ms. The simultaneous decoupling of $^{13}C'$ and ^{13}Cα/β during the T delay was achieved by the coherent adiabatic pulse decoupling, using with 10ms, 25kHz sweep width, 5.63kHz strength WURST adiabatic pulses centered at 117 ppm. Phase cycling: ϕ_1 = 2(x), 2(-x); ϕ_2 = 2(y), 2(-y); Rec. = x, -x. Pulsed field gradients $G_{1,4,5}$ are sine-bell shaped with maximum gradient strengths at their midpoints of 0.6 G/cm, 22.2 G/cm and 12.6 G/cm respectively. $G_{2,3}$ are rectangular shaped pulses with a strength of 0.6 G/cm. The durations for gradient pulses are $G_{1,2,3,4,5}$ = 10, 2.6, t_1/2, 1.0, 1.0 ms. All gradient pulses are applied along the z axis.

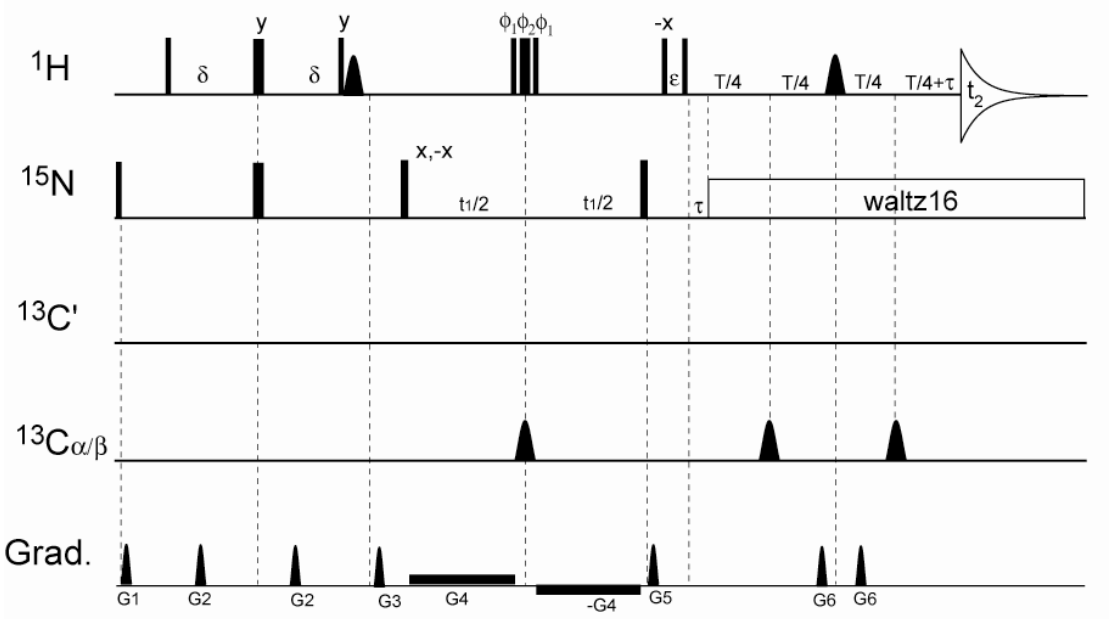

Figure S2. Pulse sequence used to measure the $^{1}H^{N}$ CSA and $^{13}C'$-$^{1}H^{N}$ dipole transverse cross-correlation rate, $\Gamma^{CSA,C'H}$. Narrow and wide pulses correspond to 90º and 180º flip angles, respectively. All ^{1}H pulses are centered on the H_2O resonance, at 4.75 ppm. The $^{13}C'/C_{\alpha/\beta}$ nuclei are decoupled by a 1.0 ms hyperbolic secant 180º pulse centered at 56.3 ppm. Protons are decoupled by the composite $90^{\circ}\phi_1$-$210^{\circ}\phi_2$-$90^{\circ}\phi_1$ pulse. The shaped ^{1}H pulse immediately following the nonselective ^{1}H 90º pulse has a flip angle of 90º and rotates the water magnetization to $-z$ while the following gradient G3 serves to prevent radiation damping until the composite 180º pulse rotates it back to $+z$. The selective 180º ^{1}H pulse prior to acquisition is of the REBURP type (1), centered at 9.05ppm, with a duration of 1.8 ms. The phases of all pulses are x unless indicated. δ = 2.6 ms, ε = 0.097 ms, τ = 5.3 ms. T was set to 2, 30, 50, 70, 90, 110, 130 and 150 ms. During the relaxation delay of T, ^{15}N is decoupled by WALTZ16 composite pulse decoupling using a RF field strength of 1.14 kHz. WALTZ16 ^{15}N decoupling with an RF field strength of 1.0 kHz is used during data acquisition. Phase cycling: $\phi_1 = 2(x), 2(-x)$; $\phi_2 = 2(y), 2(-y)$; Rec. = x, $-x$. Pulsed field gradients $G_{1,2,3,5,6}$ are sine-bell shaped with maximum gradient strengths at their midpoints of 1.2, 1.2, 24.6, 18.6 and 1.02 G/cm respectively. G_4 are rectangular shaped pulses with a strength of 0.6 G/cm. Gradient pulse durations: $G_{1,2,3,4,5,6}$ = 10, 2.4, 1.0, $t_1/2$, 0.5, 3.0 ms. All gradient pulses are applied along the z axis.

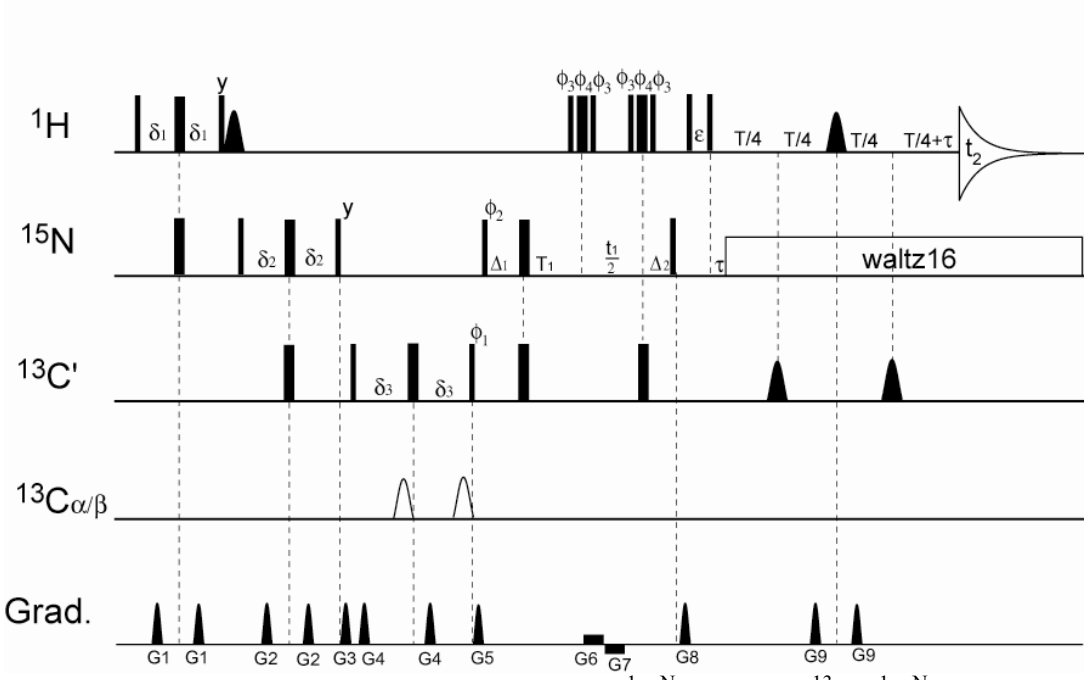

Figure S3. Pulse sequence used to measure the $^{1}H^{N}$ CSA and $^{13}C^{\alpha}$-$^{1}H^{N}$ dipole transverse cross-correlation rate, $\Gamma^{CSA,\ HC\alpha i}$ ($C_{\alpha i}$ denotes C^{α} of intra residue) and $\Gamma^{CSA,\ HC\alpha i-1}$ ($C_{\alpha i-1}$ denotes C^{α} of preceding residue). Narrow and wide pulses correspond to 90º and 180º flip angles, respectively. All the ^{1}H pulses are centered on the H_2O resonance, at 4.75 ppm. The shaped pulses applied to $^{13}C'$($^{13}C_{\alpha/\beta}$) nuclei are a 1.0 ms hyperbolic secant 180º pulse centered at 175(54.3) ppm at 600 MHz field. Protons are decoupled by the composite 90ºϕ_1-210ºϕ_2-90ºϕ_1 pulse. The shaped ^{1}H pulse immediately following the nonselective ^{1}H 90º pulse has a flip angle of 90º and rotates the water magnetization to +*z*. The selective 180º ^{1}H pulse prior to acquisition is of the REBURP type (1), centered at 9.05ppm, with a duration of 1.8 ms. The phases of all pulses are *x* unless indicated. The two shaped $^{13}C^{\alpha/\beta}$ pulses are applied (removed) to yield an anti-phase (in-phase) ^{1}H-^{15}N HSQC spectrum with respect to the sequential $^{13}C_{\alpha}$. Delays: δ_1 = 2.6 ms, δ_2 = 12.5 ms, δ_3 = 4.7 ms, ε = 0.097 ms, τ = 5.3 ms, Δ_1 = max(0, T_1-t_1/2); Δ_2 = max(0, t_1/2-T_1). T was set to 2, 30, 50, 70, 90, 110, 130 and 150 ms. During the T relaxation delay and acquisition period, ^{15}N WALTZ16 decoupling is used in the same way as described for Figure S2. Phase cycling: ϕ_1 = 2(*x*), 2(-*x*) for the in-phase spectrum and 2(*y*), 2(-*y*) for the anti-phase spectrum; ϕ_2 = (*y*), (-*y*); ϕ_3 = 2(*x*), 2(-*x*); ϕ_4 = 2(*y*), 2(-*y*); Rec. = *x*, -*x*. Pulsed field gradients, $G_{1,2,3,4,5,8,9}$ are sine-bell shaped with maximum gradient strengths at their midpoints of 7.8, 6.6, 12.0, 12.6, 18.6, 16.2 and 0.78 G/cm respectively. $G_{6,7}$ are rectangular shaped pulses with a strength of 0.3 and -0.3 G/cm. Gradient pulse durations: $G_{1,2,3,4,5,6,7,8,9}$ = 1.9, 2.4, 1.0, 0.7, 0.8, t_1/4, t_1/4, 0.2, 4.0 ms. All gradients are applied along the *z* axis.

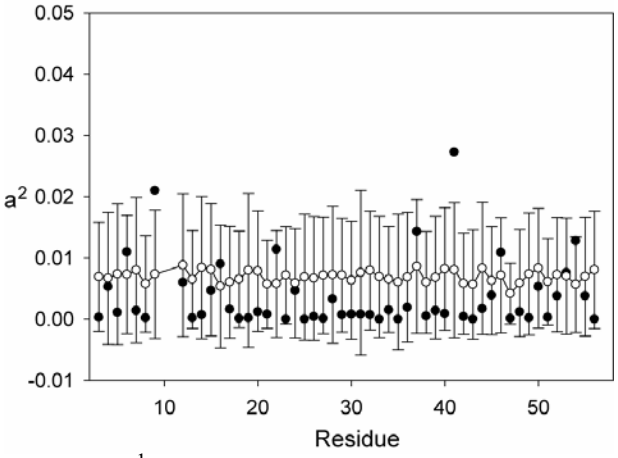

600 MHz ^{1}H frequency SECONDA analysis of ^{15}N-^{1}H RDCs in the 6 GB3 mutants. The figure shows the cumulative sum of heterogeneous modes for individual residues. Filled symbols are the a^2 values obtained when using the experimental RDCs; open symbols are the corresponding numbers for simulated RDCs to which 0.5 Hz Gaussian noise has been added, with the error bars reflecting the standard deviation of a^2 of the simulated data. Most a^2 values obtained for experimental data are within one standard deviation of the simulated a^2 values, except for G41 which was excluded from the SVD analysis. The experimental a^2 of G9 falls only slightly above the error bar and is included in the SVD analysis.

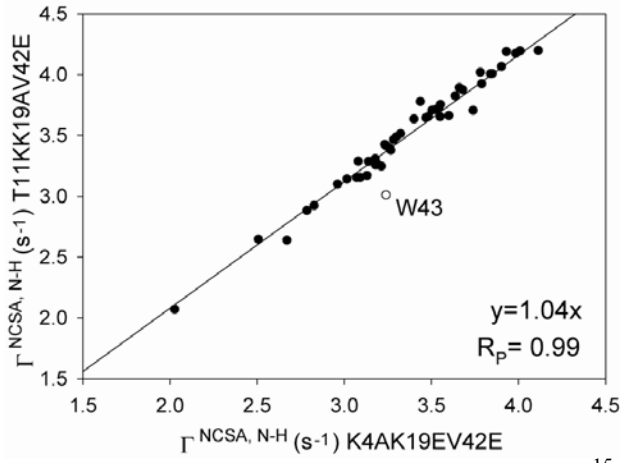

Figure S5. Comparison of the transverse ^{15}N CSA ^{15}N-^{1}H dipolar cross-correlated relaxation rates measured at 600 MHz for mutants K4A K19E V42E and T11K K19A V42E. The high Pearson's correlation coefficient of 0.99 indicates that the diffusion tensor orientation and asymmetry are very similar for the two mutants; the slope of 1.04 indicates the rotational correlation time of T11K K19A V42E is ~4% longer than that of the K4A K19E V42E mutant. W43 is an outlier and not included in the fitting.

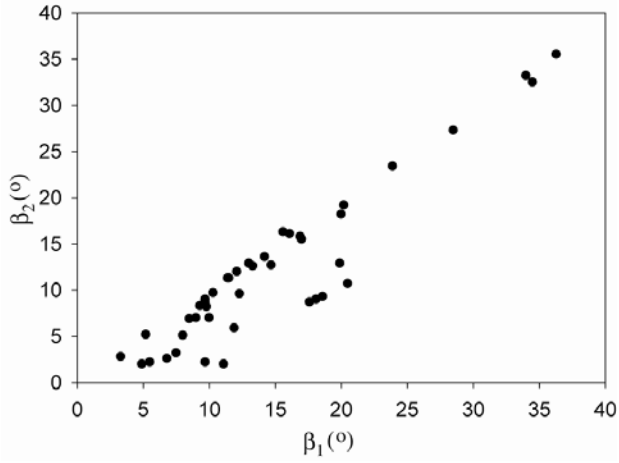

Figure S6. Correlation between β_1 and β_2 angles, defined in Fig. 5 of the main text. The strong linear correlation between the two angles (R_P = 0.93) is caused by σ_{ZZ} being nearly orthogonal to the peptide plane.

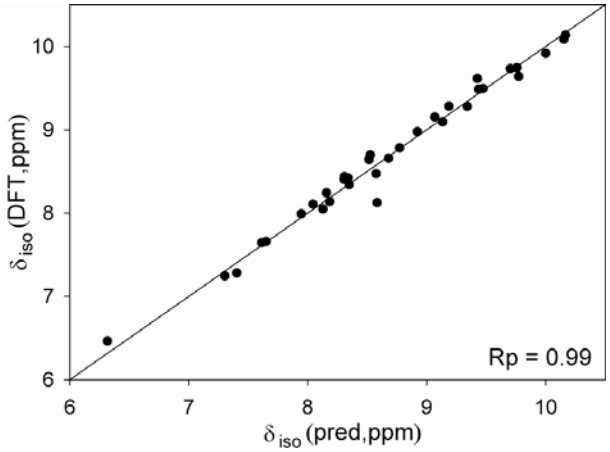

Figure S7. Correlation between DFT-calculated δ_{iso} values for NMA-acetamide pairs for H-bond geometries found in GB3 and the values obtained from the best-fitted equation $\delta_{iso}(\theta_1,\alpha_3,d_{OH}) = \left\{76.9\cos^2\theta_1 + \left[39.1\cos^2\alpha_3 + 1.8\cos\alpha_3 + 47.2\right]\sin^2\theta_1\right\}\times\exp(-1.5d_{OH}) + 5.10\,ppm.$

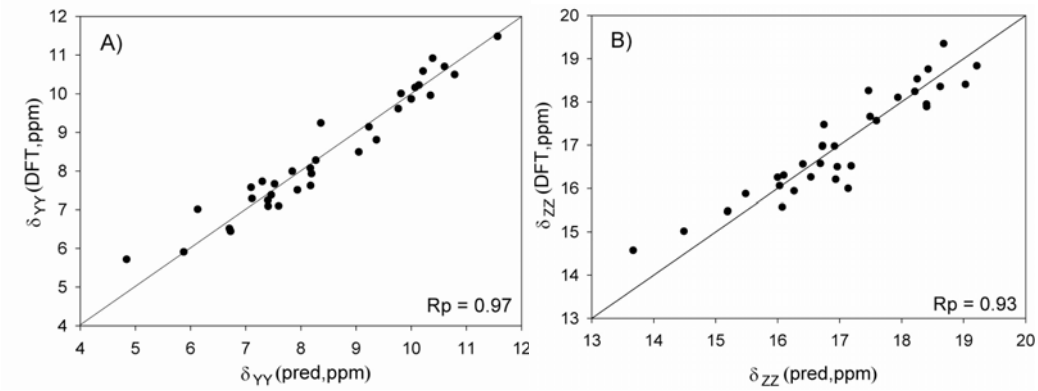

Figure S8. Correlation between DFT-calculated and the corresponding best-fitted values using eqs 3 and 4 for (A) δ_{YY} and (B) δ_{ZZ}.

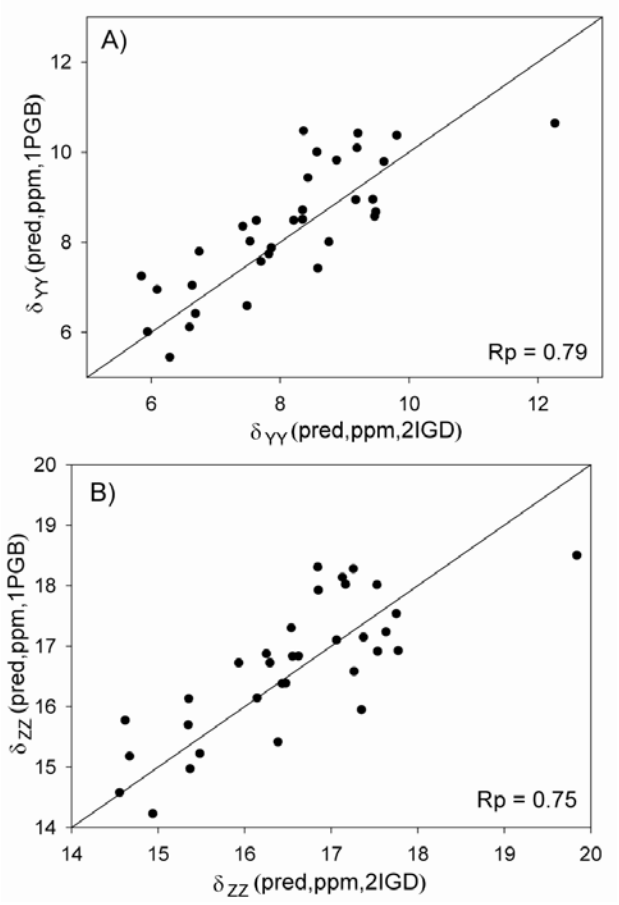

Figure S9. Correlations between (A) δ_{YY}, and (B) δ_{ZZ} values predicted for two different X-ray structures, PDB entries 1PGB and 2IGD. In both cases, hydrogen atom positions were added by the program REDUCE (2). Predicted values were obtained using eq 3 (for δ_{YY}) and eq 4 (for δ_{ZZ}). The pairwise RMSD is 0.87 ppm (A) and 0.73 ppm (B).

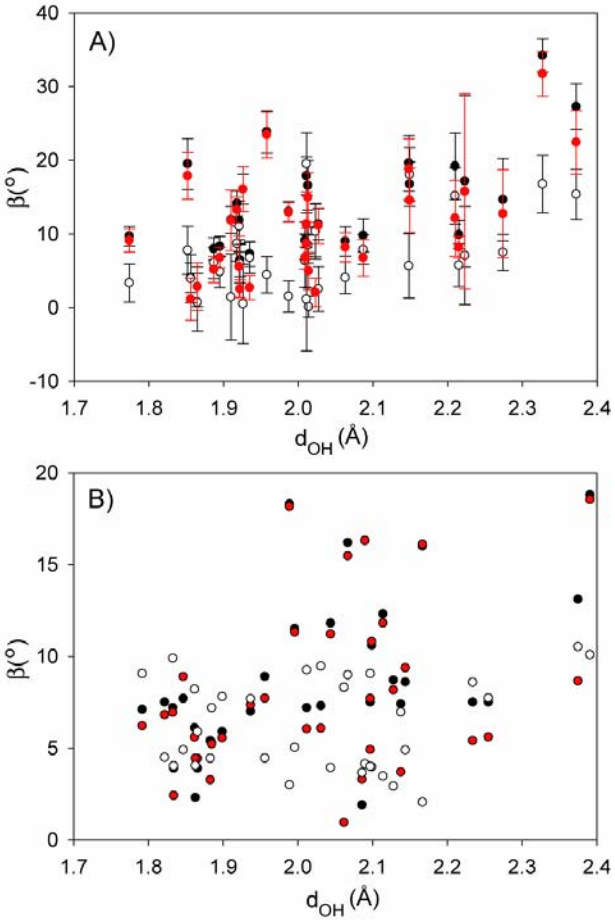

600 MHz ^{1}H frequency Correlation between β_1 (filled black circle), β_2 (filled red circle) and β_3 (empty black circle) and the hydrogen bond length d_{OH} from experimental fitting (A) and DFT calculation (B).

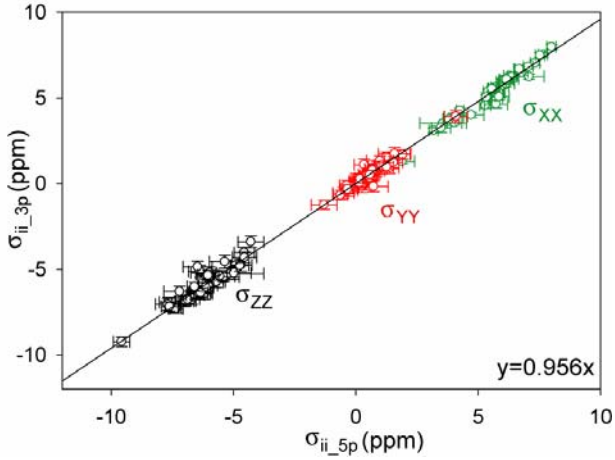

Figure S11. Comparison of σ_{ii} values determined from three-parameter (*y* axis) and five-parameter (x axis) fitting of the CSA tensor.

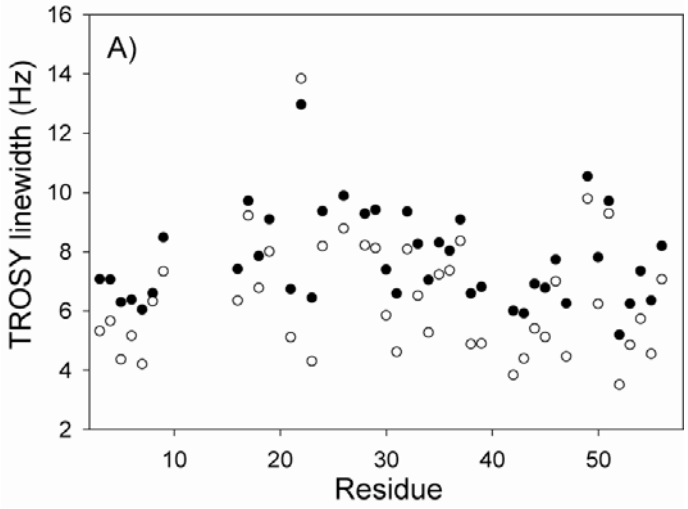

Figure S12. Calculated TROSY line widths for ^{1}H nuclei in GB3, for isotropic rotational diffusion with a correlation time of 50 ns, assuming idealized two-spin approximations for each amide group (i.e., ignoring the presence of other spins and relaxation mechanisms other than ^{1}H CSA and ^{15}N-^{1}H dipolar), using experimentally derived CSA tensors and uniform $\boldsymbol{S}^2$ = 0.903 values. Residue-specific ^{1}H TROSY line widths are calculated for magnetic field strengths corresponding to ^{1}H frequencies of 600 MHz (filled symbols) and 900 MHz (open symbols).

Table S1. Experimental $^{1}H^{N}$ RCSA values for the six GB3 mutants.[a]

residue	Mutant 1	Mutant 2	Mutant 3	Mutant 4	Mutant 5	Mutant 6
3	0.2	2.6	3.8	1.3	2.8	4.5
4	2.9	8.9	2.2	1.1	3.9	2.9
5	-4.1	4.2	2.7	1.3	-4.2	4.4
6	6.0	4.6	-1.8	2.0	0.9	-1.7
7	-5.5	-0.4	3.0	4.0	-4.5	4.1
8	8.6	-2.8	-4.9	-0.1	-1.9	-5.6
9	-6.1	1.8	3.2	3.4	-3.6	5.2
10	4.2	-6.6	N/A[b]	0.3	2.4	-4.0
11	11.3	-1.3	N/A[b]	0.0	5.6	-4.5
12	-3.0	-1.2	2.7	-1.4	-6.9	0.1
13	0.2	3.8	3.2	7.0	5.2	4.4
14	-2.9	1.2	0.3	-0.7	-3.0	1.3
15	-0.3	3.6	-0.1	0.7	-2.3	0.8
16	9.1	2.6	-2.2	2.4	2.3	-1.4
17	-5.9	4.0	3.8	-0.5	-0.6	3.8
18	8.8	6.5	-0.9	4.8	11.1	-1.1
19	-1.7	5.6	3.4	1.0	3.1	4.2
20	4.4	0.1	0.2	5.9	10.5	0.6
21	6.6	2.5	1.4	7.5	13.4	1.9
22	-8.4	2.2	2.4	-3.3	-5.8	2.7
23	-5.6	7.8	3.8	1.6	4.3	4.1
24	-10.2	-8.2[c]	2.4	1.6	N/A[b]	0.8
25	-7.8	8.1	2.0	-5.0	N/A[b]	3.2
26	-2.4	2.9	1.2	-0.2	3.8	1.1
27	-10.8	3.4	3.6	-0.1	-4.9	4.2
28	-5.0	3.8	0.2	5.7	2.5	0.1
29	-8.7	0.5	2.3	-4.7	-0.4	3.4
30	0.7	3.9	0.5	1.1	6.4	0.8
31	-12.2	1.1	1.0	-3.7	-4.8	0.7
32	-5.7	2.6	2.7	-1.5	0.9	2.5
33	-7.3	-0.4	0.8	0.3	1.1	2.9
34	-8.0	6.4	1.9	-3.9	-2.4	1.9
35	-9.1	-3.3	-0.6	-2.4	-0.4	-0.4
36	-11.5	2.3	2.4	-4.8	-4.4	3.4
37	N/A[b]	4.6	-1.3	-0.6	N/A[b]	1.3
38	4.9	-7.5	-6.2	-4.4	-5.2	-7.2
39	-1.6	-0.3	-1.2	-6.3	-3.1	-1.6
40	3.4	-3.3	-3.6	-6.0	-1.9	-5.9
41	3.0	6.9	-2.2	-2.2	3.2	-2.2
42	4.6	-3.2	-0.8	2.7	7.5	-2.8
43	-0.8	-3.8	-1.9	-1.3	-4.3	-3.1
44	-2.9	5.4	4.0	8.6	0.8	5.9
45	-4.2	3.2	2.4	1.1	-5.7	3.9
46	3.0	6.1	6.6	13.7	7.3	8.1
47	-2.1	-1.1	-0.5	-1.9	-6.7	0.2
48	1.7	-3.2	0.0	-3.1	-3.6	-1.6
49	-6.2	2.4	1.7	0.1	-5.0	2.2
50	9.3	4.8	3.1	11.1	11.3	3.8
51	-7.3	5.7	2.9	0.2	-0.4	4.4
52	0.7	5.2	4.7	4.7	-3.2	5.7
53	-1.9	3.3	0.1	0.7	-4.1	0.7

54	-5.1	-2.0	4.7	5.8	-2.2	4.2
55	1.8	-2.3	-3.1	-0.7	-2.3	-3.1
56	-5.7	-2.0	2.6	4.5	-0.8	3.7

[a] mutant 1: K19AV42ED47K; mutant 2: K19ED40NV42E; mutant 3: K4AK19EV42E-cHistag; mutant 4: K4AK19EV42E-nHistag; mutant 5: T11KK19AV42E; mutant 6: K4AK19EV42E. RCSA values are in ppb, and have been corrected for temperature and reference offset.

[b] Due to overlap (E24, T25), missing signal (K10, T11) or partially $^{1}H^{N}$-$^{1}H^{N}$ splitting (N37), RCSAs could not be measured accurately.

[c] apparent outlier; an artificially large error (1000 ppb) was added in the final fit and error analysis to effectively eliminate the impact of this data point..

Table S2. The RCSA of $^{13}C'$ of six GB3 mutants.[a]

residue	Mutant 1	Mutant 2	Mutant 3	Mutant 4	Mutant 5	Mutant 6
2	114	17	-25	63	125	-23
3	-2	-28	39	88	17	30
4	192	-12	-37	63	122	-45
5	-102	2	71	70	12	81
6	178	-25	-50	10	61	-67
7	-86	37	53	60	64	75
8	119	-38	-60	-31	20	-84
9	127	62	N/A[b]	118	92	41
10	-172	-40	N/A[b]	-48	-90	16
11	105	35	17	113	130	26
12	60	-14	-58	-68	-39	-71
13	112	-2	8	103	129	8
14	105	-13	1	96	92	5
15	-112	-7	59	49	-23	68
16	79	-31	23	108	59	17
17	-109	-12	43	0	-113	47
18	67	-28	8	106	43	10
19	-81	-37	-25	-127	-127	-29
20	-12	-26	13	-42	-112	2
21	69	-32	-31	54	83	-38
22	46	-28	9	119	89	12
23	53	51	11	-15	N/A[b]	9
24	70	-57	-34	25	N/A[b]	-53
25	-52	9	22	-41	-122	21
26	122	-19	-25	61	141	-28
27	-20	4	18	23	-85	23
28	102	-20	-45	-31	63	-58
29	-58	-41	25	34	-77	27
30	124	56	2	43	108	3
31	14	-62	-17	43	-4	-20
32	33	36	4	-34	-30	1
33	36	-47	3	76	67	3
34	42	55	16	6	-39	17
35	80	-63	-31	16	74	-52
36	N/A[b]	-12	32	-28	N/A[b]	36
37	6	77	39	75	126	55
38	26	-67	-31	9	-38	-40
39	-75	-13	21	-5	32	24
40	-39	-66	-16	-25	-80	-38
41	-36	-71	-29	-71	-139	-38
42	142	65	32	122	135	37
43	67	-31	-72	-90	-36	-84
44	174	-15	-22	97	134	-29
45	18	-4	-64	-86	-27	-69
46	102	-17	14	116	112	5
47	-51	77	20	2	4	34
48	114	-56	-49	-7	47	-66
49	-177	-10	-9	-128	-164	7
50	117	-30	-17	114	89	-8
51	63	-5	-64	-40	30	-69

52	65	18	48	130	123	50
53	145	-17	-59	-28	20	-73
54	-7	43	64	117	109	71
55	168	-2	-47	12	58	-52

[a] Mutant 1: K19AV42ED47K; mutant 2: K19ED40NV42E; mutant 3: K4AK19EV42E-cHistag; mutant 4: K4AK19EV42E-nHistag; mutant 5: T11KK19AV42E; mutant 6: K4AK19EV42E; RCSA values are in ppb, and have been corrected for temperature and reference offset. The estimated RCSA error (based on the 5th and 6th principal components of SVD analysis) is 3 ppb.
[b]Due to overlap (E24, T25), missing signal (K10, T11), or partially resolved $^{1}H^{N}$-$^{1}H^{N}$ splitting (N37), RCSAs could not be measured accurately.

Table S3. The $^{1}H^{N}$-CSA, H-X cross correlation rates, $\Gamma^{CSA,HN}$, $\Gamma^{CSA,HC'}$, $\Gamma^{CSA,HC\alpha i}$ and $\Gamma^{CSA,HC\alpha i-1}$ [a].

residue	$\Gamma^{CSA,HN}$ (s^{-1})	$\Gamma^{CSA,HC'}$ (s^{-1})	$\Gamma^{CSA,HC\alpha i}$ (s^{-1})	$\Gamma^{CSA,HC\alpha i-1}$ (s^{-1})
3	1.63	-0.22	-0.42	0.05
4	1.64	-0.34	-0.43	-0.03
5	1.79	-0.37	-0.33	-0.02
6	2.02	-0.31	-0.53	-0.01
7	1.93	-0.42	-0.31	-0.04
8	2.19	-0.49	-0.59	-0.10
9	1.38	-0.41	-0.23	-0.06
10	1.80	-0.27	-0.39	0.04
11	1.66	-0.61	-0.64	0.13
12	0.79	-0.01	-0.34	0.02
13	1.71	-0.33	-0.41	0.01
14	1.24	-0.33	-0.20	-0.05
15	1.44	-0.26	-0.35	0.03
16	1.63	-0.43	-0.42	-0.07
17	0.98	-0.10	-0.40	-0.01
18	1.52	-0.43	-0.29	-0.07
19	1.05	-0.21	-0.27	-0.02
20	1.46	-0.37	-0.34	-0.08
21	1.78	-0.30	-0.38	-0.01
22	0.38	-0.20	-0.18	-0.14
23	1.84	-0.33	-0.34	-0.02
24	1.14	-0.29	-0.25	-0.05
26	0.95	-0.21	-0.27	-0.07
28	1.19	-0.27	-0.32	-0.01
29	1.12	-0.21	-0.28	-0.01
30	1.73	-0.33	-0.38	-0.01
31	1.95	-0.36	-0.42	0.05
32	1.18	-0.23	-0.29	-0.01
33	1.41	-0.30	-0.30	0.00
34	1.79	-0.35	-0.38	0.02
35	1.66	-0.20	-0.48	0.02
36	1.84	-0.38	-0.51	-0.04
37	1.31	-0.23	-0.50	0.01
38	1.96	-0.33	-0.48	0.01
39	1.92	-0.28	-0.37	-0.01
40	1.64	-0.29	-0.31	-0.01
41	0.91	-0.16	-0.22	0.01

42	2.01	-0.25	-0.48	0.06
43	1.84	-0.33	-0.65	0.01
44	1.77	-0.36	-0.40	-0.05
45	1.67	-0.32	-0.36	-0.03
46	1.79	-0.30	-0.42	0.01
47	1.84	-0.36	-0.36	0.00
48	1.02	-0.26	-0.26	-0.03
49	0.77	-0.13	-0.25	-0.06
50	1.56	-0.25	-0.37	-0.01
51	1.00	-0.09	-0.42	0.03
52	2.31	-0.37	-0.53	0.01
53	1.91	-0.41	-0.41	-0.03
54	1.55	-0.28	-0.35	-0.03
55	1.84	-0.25	-0.50	0.04
56	1.40	-0.28	-0.32	-0.08

[a] Measured at 600 MHz ^{1}H frequency. The estimated measurement errors are, 0.045, 0.022, 0.022, 0.022 s^{-1} for columns 2-5.

Table S4. $^{1}H^{N}$ CSA tensor principal components and angles obtained using the five parameter fit.

residue	σ_{XX} (ppm)	σ_{XX} error (ppm)	σ_{YY}	σ_{YY} error (ppm)	σ_{ZZ}	σ_{ZZ} error (ppm)
3	6.04	0.18	-0.29	0.26	-5.75	0.34
4	6.07	0.18	0.97	0.32	-7.03	0.39
5	6.30	0.26	0.04	0.27	-6.34	0.39
6	7.34	0.20	0.33	0.29	-7.67	0.38
7	6.73	0.22	-0.02	0.29	-6.71	0.31
8	7.66	0.18	1.87	0.30	-9.54	0.33
9	5.23	0.23	0.86	0.33	-6.09	0.39
16	6.08	0.20	1.39	0.31	-7.47	0.33
17	5.42	0.47	0.63	0.29	-6.05	0.48
18	5.76	0.39	1.25	0.32	-7.01	0.41
19	4.79	0.52	0.63	0.35	-5.42	0.63
21	6.46	0.21	0.06	0.30	-6.52	0.30
22	1.83	0.52	4.04	0.47	-5.87	0.77
23	6.02	0.28	-0.57	0.44	-5.45	0.56
24	3.59	0.95	1.58	0.66	-5.16	1.39
26	3.18	0.18	1.37	0.37	-4.56	0.41
28	4.75	0.40	0.43	0.56	-5.18	0.71
29	4.09	0.30	0.22	0.38	-4.31	0.53
30	5.84	0.21	0.32	0.40	-6.16	0.33
31	6.08	0.16	-0.28	0.37	-5.80	0.38
32	3.84	0.25	0.87	0.37	-4.71	0.44
33	4.25	0.15	0.51	0.39	-4.76	0.36
34	5.72	0.18	0.31	0.37	-6.03	0.38
35	5.64	0.21	0.76	0.37	-6.39	0.45
36	6.20	0.34	1.50	0.37	-7.69	0.51
37	5.30	0.27	1.18	0.59	-6.47	0.59
38	6.38	0.18	0.17	0.29	-6.55	0.30
39	6.00	0.14	-0.30	0.35	-5.70	0.36
42	6.71	0.25	-1.33	0.53	-5.38	0.64
43	7.52	0.19	-0.27	0.24	-7.25	0.27
44	6.17	0.29	0.68	0.30	-6.85	0.33
45	6.18	0.30	0.40	0.25	-6.57	0.37
46	7.11	0.62	0.16	0.40	-7.27	0.65
47	6.82	0.26	-0.40	0.31	-6.42	0.34
49	3.50	0.39	1.08	0.26	-4.58	0.50
50	5.41	0.20	0.16	0.28	-5.57	0.30
51	5.82	0.42	0.20	0.30	-6.02	0.43
52	8.01	0.19	-0.64	0.29	-7.37	0.30
53	7.06	0.20	0.56	0.28	-7.61	0.34
54	5.57	0.17	0.59	0.30	-6.16	0.32
55	6.68	0.17	-0.36	0.29	-6.33	0.29
56	5.30	0.19	1.28	0.28	-6.58	0.31

residue	β_1 (°)	β_1 error (°)	β_2 (°)	β_2 error (°)	β_3	β_3 error (°)	β_1'(°)	ω_1(°)	ω_2(°)	ω_3(°)
3	16.1	2.3	16.1	3.8	1.0	7.7	16.1	-14.4	-1.0	-1.6
4	9.3	1.9	8.3	1.9	4.5	2.8	8.2	-18.5	-4.5	10.2

5	3.3	1.6	2.8	3.0	1.8	4.2	2.8	-4.0	-1.8	1.2
6	14.2	1.5	13.6	1.6	8.9	2.3	12.1	-45.5	-8.9	33.1
7	4.9	1.5	2.0	3.2	5.2	3.5	-0.9	-20.1	-5.2	20.9
8	8.0	2.0	5.1	1.9	6.3	2.2	5.1	-5.0	-6.2	-0.1
9	15.6	2.3	16.3	5.0	19.0	3.9	-10.2	-42.6	-19.0	51.2
16	10.0	2.8	7.0	2.4	8.2	2.1	6.3	-23.0	-8.2	16.6
17	34.0	2.4	33.2	2.7	18.7	3.5	30.0	-56.2	18.7	25.0
18	11.1	2.9	2.0	2.0	10.9	4.1	-2.0	0.3	-10.9	1.7
19	17.6	3.8	8.7	3.0	19.0	4.9	4.6	23.4	-19.0	-26.7
21	12.3	2.0	9.6	2.0	7.7	2.0	9.7	-1.6	-7.7	-8.0
22	18.6	10.6	9.3	9.2	16.4	6.4	-9.7	-3.2	16.3	12.3
23	5.5	1.7	2.2	6.4	5.3	6.1	-2.0	-11.1	5.2	13.0
24	10.3	32.5	9.7	22.3	3.5	10.7	9.7	-3.2	-3.6	-6.5
26	14.7	6.9	12.7	5.8	7.7	3.7	12.6	-16.8	-7.7	4.1
28	20.5	8.2	10.7	4.8	17.8	6.1	11.2	2.4	-17.8	-12.9
29	19.9	4.1	12.9	5.4	16.0	4.3	12.2	-19.7	-15.9	7.2
30	11.9	2.4	5.9	5.4	11.1	4.0	4.8	-17.2	11.1	12.1
31	8.5	1.4	6.9	1.9	4.8	3.2	7.0	-4.2	-4.9	-2.7
32	20.2	4.3	19.2	4.2	6.3	4.4	19.3	-13.9	-6.2	-5.3
33	5.2	2.5	5.2	3.2	0.1	3.1	5.2	-12.6	-0.1	7.4
34	6.8	1.8	2.6	1.6	6.3	3.1	2.6	0.7	-6.3	-3.3
35	23.9	3.0	23.4	3.4	4.6	3.4	23.5	-13.3	-4.6	-10.2
36	20.0	2.9	18.2	3.0	8.6	3.6	18.2	-18.8	-8.6	0.6
37	28.5	3.3	27.3	4.2	8.3	5.0	27.4	-20.4	-8.3	-6.9
38	9.8	1.7	8.2	1.7	5.5	2.6	8.2	3.7	5.5	-11.9
39	12.1	1.6	12.0	1.6	1.8	2.3	12.0	-16.8	-1.9	4.8
42	11.4	1.9	11.3	4.9	1.3	7.5	11.3	2.0	1.3	-13.3
43	13.3	1.2	12.6	2.0	4.4	3.8	12.5	-22.0	4.5	9.4
44	9.0	2.0	7.0	1.9	6.2	4.0	6.9	12.6	6.2	-19.3
45	9.7	1.5	8.7	1.5	4.3	3.7	8.6	-9.6	-4.3	1.0
46	18.1	3.4	9.0	2.1	19.8	3.9	4.2	24.2	-19.8	-27.0
47	9.7	1.6	2.2	1.5	9.5	3.2	2.2	1.5	-9.5	-3.6
49	36.3	5.7	35.5	5.8	7.6	5.0	35.7	-6.1	-7.6	-29.4
50	17.0	2.3	15.5	2.6	7.2	3.5	15.5	-14.4	7.2	-1.1
51	34.5	2.2	32.5	3.1	17.0	4.3	30.9	-48.0	-17.0	16.4
52	9.7	1.5	9.0	1.4	3.7	2.7	9.0	-13.4	-3.8	4.5
53	7.5	1.7	3.2	2.1	7.0	2.4	2.8	-12.8	-7.0	9.9
54	11.5	2.7	11.3	3.2	2.5	3.4	11.2	-13.9	2.5	2.7
55	13.0	1.5	12.9	1.9	1.2	4.5	12.9	-6.1	1.2	-6.9
56	16.9	3.5	15.8	3.5	8.5	2.5	14.9	-37.7	8.5	22.5

Table S5. The DFT-calculated $^{1}H^{N}$ CSA tensor components for NMA-acetamide pairs with geometries found in PDB entry 2OED.

residue	δiso(ppm)	δ_{ZZ}(ppm)	δ_{YY}(ppm)	δ_{XX}(ppm)
3	10.16	19.22	10.39	0.86
4	8.35	16.94	7.12	1.00
5	9.78	19.03	10.22	0.08
6	9.07	17.60	9.24	0.38
7	9.34	18.41	9.82	-0.19
8	10.00	18.26	10.79	0.96
9	8.59	17.14	6.13	2.48
14	8.68	16.73	8.18	1.14
16	9.19	18.41	8.37	0.80
18	8.78	16.73	9.05	0.55
20	8.31	16.00	7.94	0.98
26	7.65	15.20	6.73	1.03
27	9.71	18.43	10.61	0.08
28	7.95	15.49	7.60	0.76
29	7.62	15.20	6.71	0.95
30	9.43	17.47	10.35	0.46
31	10.17	18.68	11.57	0.26
32	8.05	16.03	7.47	0.64
33	8.52	16.92	8.28	0.36
34	9.48	18.22	10.08	0.14
35	8.31	16.69	7.85	0.39
36	9.44	17.94	10.00	0.37
37	6.32	13.67	4.85	0.44
38	7.41	16.08	7.41	-1.27
39	9.14	17.50	9.77	0.14
42	8.92	16.75	9.37	0.65
44	8.34	16.97	7.10	0.96
46	8.16	16.54	7.30	0.64
51	7.31	14.49	5.88	1.54
52	9.76	18.63	10.14	0.51
53	8.19	16.10	8.18	0.28
54	8.53	16.41	8.20	0.98
55	8.58	17.19	7.53	1.02
56	8.13	16.27	7.41	0.71

Table S6. Fitted $^{1}H^{N}$ CSA values using the three-parameter model

residue	σ_{XX} (ppm)	σ_{XX} error (ppm)	σ_{YY}	σ_{YY} error (ppm)	σ_{ZZ}	σ_{ZZ} error (ppm)	β_1'(°)	β_1' error (°)
3	6.07	0.18	-0.30	0.23	-5.77	0.30	16.4	1.7
4	5.99	0.14	0.84	0.29	-6.83	0.31	8.2	1.6
5	6.30	0.14	0.03	0.25	-6.33	0.26	2.8	1.5
6	7.04	0.15	-0.14	0.24	-6.90	0.28	11.7	1.3
7	6.62	0.14	0.13	0.29	-6.75	0.31	-0.2	1.4
8	7.52	0.12	1.67	0.28	-9.20	0.28	6.7	1.9
9	4.57	0.16	0.71	0.33	-5.28	0.26	-5.4	2.8
16	5.70	0.13	1.46	0.30	-7.17	0.30	7.7	2.7
17	4.85	0.22	0.54	0.23	-5.39	0.35	32.7	2.5
18	5.29	0.15	1.54	0.29	-6.83	0.28	0.9	2.7
19	4.01	0.15	0.52	0.36	-4.53	0.38	10.1	2.8
21	6.15	0.14	0.31	0.29	-6.46	0.28	7.0	1.8
22	1.30	0.13	3.94	0.35	-5.24	0.34	-1.7	3.7
23	5.95	0.13	-0.57	0.33	-5.38	0.33	-2.0	1.3
24	3.52	0.13	1.72	0.38	-5.25	0.35	12.1	4.7
26	3.10	0.14	0.89	0.33	-3.99	0.31	10.7	4.0
28	3.98	0.21	1.30	0.28	-5.28	0.38	25.8	4.1
29	3.56	0.12	-0.15	0.37	-3.41	0.35	7.0	2.6
30	5.32	0.12	1.07	0.34	-6.39	0.35	1.4	2.0
31	5.97	0.13	-0.41	0.36	-5.56	0.34	6.2	1.3
32	3.75	0.18	0.92	0.30	-4.67	0.35	20.1	4.0
33	4.26	0.14	0.49	0.36	-4.75	0.32	5.6	2.1
34	5.64	0.12	0.28	0.36	-5.91	0.35	2.7	1.7
35	5.52	0.18	0.79	0.32	-6.30	0.38	23.9	2.7
36	5.83	0.15	1.20	0.36	-7.03	0.34	14.8	2.4
37	5.15	0.18	0.87	0.30	-6.02	0.34	27.5	2.8
38	6.26	0.14	0.10	0.29	-6.36	0.27	7.1	1.5
39	6.00	0.13	-0.29	0.33	-5.71	0.33	11.9	1.5
42	6.69	0.15	-1.26	0.27	-5.43	0.25	11.3	1.3
43	7.49	0.15	-0.21	0.23	-7.28	0.27	13.1	1.1
44	6.01	0.14	0.75	0.29	-6.76	0.26	6.4	2.1
45	6.07	0.15	0.43	0.23	-6.50	0.27	7.9	1.5
46	6.25	0.16	0.04	0.30	-6.29	0.30	13.5	2.0
47	6.49	0.14	-0.14	0.29	-6.35	0.31	4.0	1.4
49	3.24	0.26	1.03	0.22	-4.27	0.31	32.3	5.3
50	5.37	0.14	0.02	0.24	-5.39	0.23	15.6	2.1
51	5.07	0.20	0.27	0.24	-5.33	0.29	31.4	1.8
52	7.98	0.15	-0.68	0.27	-7.30	0.26	10.0	1.1
53	6.83	0.14	0.33	0.26	-7.17	0.27	2.3	1.6
54	5.55	0.16	0.50	0.26	-6.04	0.27	10.3	2.0
55	6.68	0.14	-0.34	0.25	-6.34	0.26	12.9	1.5
56	5.04	0.16	0.95	0.25	-5.98	0.27	8.4	2.5

1. Geen H & Freeman R (1991) Band-selective radiofrequency pulses. *J. Magn. Reson.* 93**:** 93-141.
2. Word JM, Lovell SC, Richardson JS, & Richardson DC (1999) Asparagine and glutamine: Using hydrogen atom contacts in the choice of side-chain amide orientation. *J. Mol. Biol.* 285**:** 1735-1747.